J Appl Electrochem (2010) 40:921–932
DOI 10.1007/s10800-009-0031-z

ORIGINAL PAPER

Mathematical modeling of high-pressure PEM water electrolysis

S. A. Grigoriev · A. A. Kalinnikov · P. Millet · V. I. Porembsky · V. N. Fateev

Received: 30 November 2008 / Accepted: 29 October 2009 / Published online: 21 November 2009

Abstract This paper is devoted to the modeling and numerical optimization of proton-exchange membrane (PEM) water electrolysers for operation at elevated pressures (up to 130 bars). The model takes into account different geometrical parameters of the PEM cell, the kinetics of the hydrogen and oxygen evolution reactions, the electro-osmotic drag of water molecules, the permselectivity of the solid polymer electrolyte and associated gas cross-over phenomena. The role of various operating parameters (such as pressure, temperature, current density, flow rate of water) on cell efficiency, faradaic yield and heat produced during water electrolysis is evaluated and discussed. The model is also used for the purpose of optimizing the performances of PEM cells. In particular, optimal values of some critical operating parameters (current density, rate of water supplied to the anodes) are recommended.

Keywords Proton-exchange membrane (PEM) · Water electrolysis · High pressure · Mathematical modeling

S. A. Grigoriev (✉) · A. A. Kalinnikov · V. I. Porembsky · V. N. Fateev
Hydrogen Energy and Plasma Technology Institute of Russian Research Center "Kurchatov Institute", Kurchatov sq., 1, 123182 Moscow, Russia
e-mail: s.grigoriev@hepti.kiae.ru

S. A. Grigoriev · V. N. Fateev
Moscow Power Engineering Institute (Technical University), Krasnokazarmennaya 14, 111250 Moscow, Russia

P. Millet
Institut de Chimie Moléculaire et des Matériaux, UMR CNRS, n° 8182, Université Paris Sud, bât 420, 91405 Orsay Cedex, France

List of symbols

C_g, C_l, C_H, C_O (mol m^{-3})	Molar density of gas, liquid, hydrogen, oxygen.
$\boldsymbol{\upsilon}_g$, $\boldsymbol{\upsilon}_l$ (m s^{-1})	Velocity of gas and liquid.
υ_0 (m s^{-1})	Velocity of cooling water
P_g, P_l, P_c (Pa)	Pressure of gas, liquid and capillary pressure
K_p (m^2)	Permeability of porous current collector
R_p (m)	Average pore radius of porous current collector
k_{rl}, k_{rg}	Relative permeabilities of liquid and water
s (adim.)	Saturation of porous current collector
s_{fc} (adim.)	Saturation at the current collector–flow channel interface
s_{cl} (adim.)	Saturation at the current collector–catalytic layer interface
θ_c (deg.)	Wetting angle of porous current collector
ε (adim.)	Porosity of gas diffusion layer
R_{bc} (m)	Critical bubble radius
N_g, N_l, N (mol m^{-2} s^{-1})	Flux of gas, liquid, total flux
N_{ga}, N_{la} (mol m^{-2} s^{-1})	Gas and liquid fluxes at current collector–anodic layer interface
N_{gc}, N_{lc} (mol m^{-2} s^{-1})	Gas and liquid fluxes at current collector–cathodic layer interface
C_H (mol m^{-3})	Hydrogen concentration in the gas phase
R_p (m)	Effective pore radius

i_Σ, i_0, i_p (A m^{-2})	Total, useful, and parasitic current densities
n_p (adim.)	Electro-osmotic drag coefficient
P_s (Pa)	Pressure of saturated water vapor
h_m (m)	Membrane thickness
h (m)	Gas diffusion layer thickness
h_{fc} (m)	Flow channel thickness
ΔT (°C)	Temperature difference along the membrane-electrode assembly (MEA)
S_{MEA} (m^2)	Active area of MEA
i_{ex} (A m^{-2})	Exchange current density
ρ_m (Ohm^{-1} m^{-1})	Specific ionic conductivity of solid polymer electrolyte

Physicochemical parameters

$C_{pw} = 4{,}217$ (J kg^{-1} K^{-1})	Specific heat of liquid water at $T = 100$ °C
$\mu_l = 2.822 \times 10^{-2}$ (Pa s)	Dynamic viscosity of liquid water at $T = 100$ °C and $P = 13$ MPa
$\mu_H = 1.09 \times 10^{-5}$ (Pa s)	Dynamic viscosity of hydrogen at $T = 100$ °C and $P = 13$ MPa
$\mu_O = 2.47 \times 10^{-5}$ (Pa s)	Dynamic viscosity of oxygen at $T = 100$ °C and $P = 13$ MPa
$\sigma = 0.05884$ (Pa m)	Surface tension of water at $T = 100$ °C and $P = 13$ MPa
$\Gamma_H = 1.67 \times 10^{-3}$ (mol mol^{-1})	Water solubility of hydrogen at $T = 100$ °C and $P = 13$ MPa
$\Gamma_O = 1.85 \times 10^{-3}$ (mol/mol)	Water solubility of oxygen at $T = 100$ °C and $P = 13$ MPa
$E_{eq} = 1.29$ (V)	Equilibrium cell voltage at $T = 100$ °C and $P = 13.0$ MPa
$\Delta H° = -285.0$ (kJ/mol)	Enthalpy change for reaction $H_2 + \frac{1}{2}O_2 \rightarrow H_2O(l)$ at $T = 100$ °C

Fitted equations

$n_p = 2.3 + 0.0212 \cdot (T - 80)$	Number of solvated water molecules associated with each proton (drag factor) in solid polymer electrolyte at full humidification versus temperature T in °C (approximated from data in [1]).
$D_{OM} = 2.44 \times 10^{-8} \exp\left(-\frac{2{,}100}{T}\right)$ (m^2 s^{-1})	Diffusion coefficient of oxygen in solid polymer electrolyte at full humidification (approximated from data in [2]).
$D_{HM} = 5.65 \times 10^{-8} \exp\left(-\frac{2{,}100}{T}\right)$ (m^2 s^{-1})	Diffusion coefficient of hydrogen in solid polymer electrolyte at full humidification (approximated from data in [2]).
$F_c(s) = \begin{cases} 1.417(1-s) \\ -2.12(1-s)^2 \\ +1.263(1-s)^3 \\ \quad \text{if } \theta_c < 90^\circ \\ 1.417s \\ -2.12s^2 \\ +1.263s^3 \\ \quad \text{if } \theta_c > 90^\circ \end{cases}$	Leverett function which is used to determine capillary pressure in porous media as a function of the wetting angle θ_c (taken from [3]).
$E_r = E^{(0)} - 8.5 \times 10^{-4}(T - 298.15) + 4.308 \times 10^{-5} T \ln\left(P_H P_O^{0.5}\right)$ (V)	Reversible voltage of electrolysis cell as a function of temperature T and gas pressures.
$E_{tn} = -\frac{\Delta H^{(0)}}{2F} - 8.5 \times 10^{-4}(T - 298.15) + 4.308 \times 10^{-5} T \ln\left(P_H P_O^{0.5}\right)$ (V)	Thermoneutral voltage of electrolysis cell as a function of temperature T and gas pressures.

1 Introduction

Proton-exchange membrane (PEM) water electrolysis [4–6] offers an interesting alternative to conventional alkaline water electrolysis. High current densities (in the 1–5 A cm^{-2} range) have been reported on large (1–5 N m^3 H_2/h) PEM systems [4, 5] and high operating pressure can be reached for direct storage of hydrogen in pressurized vessels. However, different problems must be overcome to operate PEM cells under such severe operating conditions. Main factors controlling the overall performance of PEM water electrolysers are (i) the mass flow of water supplied to the anode, (ii) the rate of oxygen transport away from the anode and (iii) the electric current distribution between current collectors and catalytic layers. If a reaction zone is not properly fed with water during operation and if uneven ohmic resistances exist over the surface of the membrane-electrode assemblies (MEAs), then the current density is not homogeneously distributed and the efficiency of the electrolyser can decrease significantly. In this paper, the role of the operating pressure is more specifically considered. When water electrolysis is performed at elevated pressures, some specific advantages are obtained compared to atmospheric operation: (i) the thermoneutral voltage increases with the operating pressure, thus reducing thermal emissions during electrolysis; (ii) the relative volume of the gas phase decreases when the pressure increases and, as a result, a more efficient transport of biphasic (liquid–gas) mixtures across the porous current collectors is obtained, leading to higher kinetics. The bad news is that gas cross-permeation phenomena through the solid polymer electrolyte (SPE) increase in magnitude when the operating pressure is raised. This leads

to higher contamination levels in the gaseous production (mainly H_2 in O_2 because hydrogen diffusivity in the SPE is larger than the oxygen one, but also O_2 in H_2), and to specific hazards which have to be carefully managed (the lower limit of explosivity of H_2 in O_2 is 4 vol%). This also leads to lower current efficiencies (faradaic yield), increased ohmic and polarization losses of potential because cross-diffusion of hydrogen and oxygen generate a parasitic current analogous to an internal cell short-circuit, not leading to water decomposition. For practical applications, operating pressures up to 130 bars are targeted. They allow the direct fueling of standard industrial hydrogen (and oxygen) storage vessels. Pressures of 130 bars (2,000 psi) are also a threshold between different grades of pressure-supporting structures.

The purpose of the work presented here was to identify the most significant physical and chemical phenomena controlling the kinetics and efficiency of water decomposition at high pressure in PEM water electrolysers. A correct description of these phenomena is required to solve the engineering problems associated with the development of efficient high-pressure PEM water electrolysers. Modeling has been used for that purpose, to optimize the design of PEM cells for efficient water–gas transport and proper heat management during electrolysis. Physical and chemical models of transfer processes which cannot be treated using standard mathematical methods and which are not clearly described in the literature related to high-pressure PEM water electrolysis, are more specifically considered in this paper, namely: (i) processes of heat- and mass-transfer across porous current collectors when biphasic mixtures are involved; (ii) dynamics of gas bubbles evolution at interfaces between current collectors and flow channels. In the literature, only few papers are dealing with the modeling of PEM water electrolysers, and in most cases, the different aspects (electrode kinetics, mass-transfer in current collectors, mass-transfer and heat-transfer in flow channels) are treated separately. Onda et al. [7] provided a model to account for current–voltage relationships. The cell voltage was described by the sum of Nernstian potential, ohmic potential, and also cathodic and anode overvoltages. Empirical equations for overvoltage as function of operating temperature and current density were proposed. A similar simplified approach has been used in [8], also considering mass balance and charge on electrodes, but treatment of mass-transport effects are seldom found. The theoretical description of biphasic transport in porous media (current collector) for application in PEM fuel cells can be found in several papers [9–15]. Some works have included flooding effects as the concentrated parameter in the single-phase transport equation through the effective factor of diffusion [9, 10]. Other research papers offer models for the transport of biphasic mixtures in hydrophilic [11–15] and hydrophobic [3, 16] gas diffusion layers. In the literature, two different approaches are followed to describe the transport of biphasic media. In earlier works on fuel cell modeling, the transport of biphasic mixtures in current collectors was treated by using the well known theory of un-saturated flow (UFT) [12, 15]. That theory assumes that the pressure of a gas is constant in the porous media, and that the pressure of the liquid phase is equal to the capillary pressure. Multiphase modeling (M^2) [17] offers a more appropriate description of the problem and provide the exact reformulation of classical biphasic model in one single equation. The main difference with the UFT approach is that the condition of constant gas phase pressure is released. Another essential feature of M^2 consists in the possibility of having domains where single and double phase co-exist. In classical biphasic models, the treatment of interfaces between regions of single and double phase essentially increase the complexity of the numerical solution. Most of these aspects are considered in the present work and used to propose a model for high-pressure PEM water electrolysis. The role of various operating parameters (such as temperature, pressure, current density, flow rate of water supplied to the anode) on cell efficiency, faradaic yield and heat produced during water electrolysis is evaluated and discussed. The model is also used for the purpose of optimizing the performances of a PEM cell and optimal values of some critical parameters are recommended.

2 Modeling

2.1 Geometrical description of the PEM cell

The different components of a conventional PEM water electrolysis cell are pictured in Fig. 1. This is a composite structure. The different domains have been modeled individually and interconnected through appropriate boundary conditions.

Domain 1, 2—anodic and cathodic mass flow channels. From a geometrical viewpoint, this is a regular network of rectangular channels machined in the thickness of the bipolar plates (8 in Fig. 1). One flow channel (electronic conductor) is positioned on each side of the PEM cell. A constant mass flow of liquid water is set as boundary condition on the input side of the plates. Along the channels, biphasic mixtures of liquid water, gaseous hydrogen (cathode) or gaseous oxygen (anode) and water vapor are formed during electrolysis. Mixtures of constant composition are set as boundary conditions on the exit sides of the cell.

Domain 3, 4—anodic and cathodic current collectors. Two porous current collectors (electronic conductors) made of sintered titanium particles are then placed on each

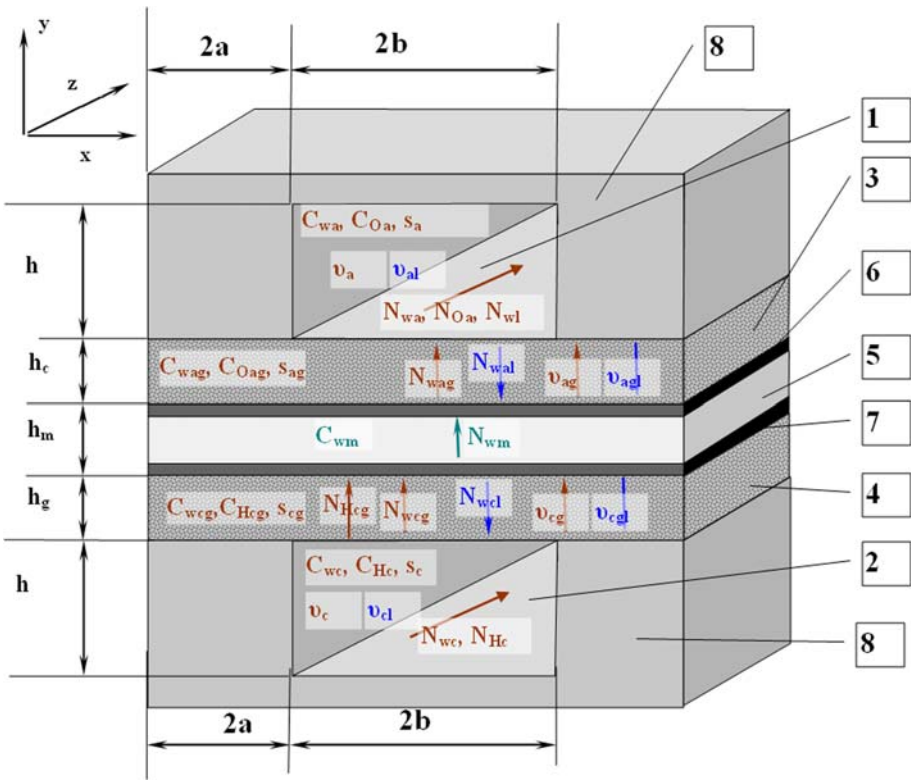

Fig. 1 Schematic diagram of cell components. *1* Anode flow-field channel, *2* cathode flow-field channel, *3* anode current collector, *4* cathode current collector, *5* solid polymer electrolyte membrane, *6* cathode electrocatalytic layer, *7* anode electrocatalytic layer, *8* current transfer rib of bipolar plate

side of the PEM cell. The surface of the current collectors (x–z plane) is in direct contact with the surface of the bipolar plates (no interface ohmic drop). The two-phase mixtures of liquid water, gaseous hydrogen (oxygen) and water vapor flow across the structure, along the y axis (perpendicular to the surface). Capillary forces are motive forces to the transfer.

Domain 5—membrane. This is the proton-conducting solid polymer electrolyte (SPE). Both protons and water molecules are transferred from the anode to the cathode, across the membrane thickness, during water electrolysis. The flow of water is caused by diffusion and by the electro-osmotic drag (solvated protons are migrating to the cathode and solvation water molecules taken at the anode are released at the cathode).

Domain 6—anodic catalytic layer. Water oxidation takes place at the interface between the anodic catalyst and the SPE, leading to the formation of protons, electrons and gaseous oxygen:

$$2H_2O \rightarrow 4H^+ + 4e^- + O_2$$

This is the catalytic layer (a mixture of percolating catalytic particles, SPE and pores) which is typically a few microns thick (3D interface). Electrons are collected through the current collectors and bipolar plates. Gaseous oxygen formed by the oxygen evolution reaction (OER) is released across the porous current collector and protons are transferred to the cathode by migration across the SPE.

Domain 7—cathodic catalytic layer. Protons reduction into gaseous hydrogen (hydrogen evolution reaction or HER) takes place in the cathodic catalytic layer according to:

$$4H^+ + 4e^- \rightarrow 2H_2$$

The catalytic layer has the same structure than the anodic one, the only main difference being the kind of catalyst used for the HER (platinum) compared to the catalyst used for the OER (iridium or its oxides). Electrons reach the reaction sites from the external circuit and the cathodic current collectors; protons are transferred from the membrane.

2.2 Simplifying assumptions

The model presented here is based on the following simplifying assumptions:

- all physical processes are taking place at constant pressure and temperature;
- gases formed at the electrodes and transferred to the anodic and cathodic channels are ideal gases;
- porous current collectors have isotropic properties and interfaces with adjacent regions are planar and free from parasitic ohmic drops.

2.3 Governing equations and boundary conditions

The most significant physicochemical processes which have to be considered for modeling high-pressure water electrolysers are now described and the corresponding equations are presented.

2.3.1 Equations used to model the transport of liquid and gas phases across the hydrophilic porous current collectors

General equations describing the transport of two-phase mixtures are derived from the general laws of mass and momentum conservation for gas and liquid phases. Mass conservation of gas phase in the absence of the gas source is expressed by:

$$\nabla\left(C_{\mathrm{g}}\boldsymbol{\upsilon}_{\mathrm{g}}\right)=0 \tag{1}$$

$C_g\boldsymbol{\upsilon}_g$ is the total flux of the gas phase. Assuming $C_{\mathrm{g}}=\text{const}$ (for example during operation at constant current density), Eq. 1 may be rewritten as:

$$\nabla\boldsymbol{\upsilon}_g=0. \tag{2}$$

In a similar way, mass conservation of the liquid phase can be expressed as follows:

$$\nabla\boldsymbol{\upsilon}_{\mathrm{l}}=0. \tag{3}$$

Momentum conservation of gas and liquid phases can be expressed by equating the resisting forces to pressure gradients for each individual phase [3]. For the gas phase, this leads to:

$$\nabla P_{\mathrm{g}}=-\lambda_{\mathrm{g}}\upsilon_{\mathrm{g}}\quad \lambda_{\mathrm{g}}=\frac{\mu_{\mathrm{g}}}{K_{\mathrm{p}}k_{\mathrm{rg}}}=\frac{\mu_{\mathrm{g}}}{K_{\mathrm{p}}(1-s)^3} \tag{4}$$

for the liquid phase, one obtains:

$$\nabla P_{\mathrm{l}}=-\lambda_{\mathrm{l}}\upsilon_{\mathrm{l}}\quad \lambda_{\mathrm{l}}=\frac{\mu_{\mathrm{l}}}{K_{\mathrm{p}}k_{\mathrm{rl}}}=\frac{\mu_{\mathrm{l}}}{K_{\mathrm{p}}s^3}. \tag{5}$$

Equations 4 and 5 are the expressions of Darcy's law for each phase. In the case under consideration, Darcy's law can be used for gases and liquids because only laminar flows are considered (see discussion in [3]). In the present case, the Reynolds number in the porous current collector is:

$$\mathrm{Re}=\frac{\upsilon_{\mathrm{g}}d_{\mathrm{pore}}}{\nu_{\mathrm{g}}}\approx\frac{\rho_{\mathrm{g}}\upsilon_{\mathrm{g}}\sqrt{K}}{\mu_{\mathrm{g}}}=\frac{N_{\mathrm{g}}}{A_{\mathrm{g}}\mu_{\mathrm{g}}}\sqrt{K}\approx\frac{I}{2A_{\mathrm{g}}\mu_{\mathrm{g}}F}\sqrt{K}$$
$$\approx\frac{10^4\times10^{-6}}{2\times0.002\times2\times10^{-5}\times10^5}\approx1.25,$$

where μ is dynamic viscosity, A is the molar weight of gas (kg mol^{-1}), K is the permeability, ν is the kinematic viscosity. Thus, Re is close to unity and hence, even at the cathode (hydrogen), the flow in the porous current collector is laminar, and Darcy's law applies. The difference of pressure $P_{\mathrm{g}}-P_{\mathrm{l}}$ is equal to the capillary pressure P_{c}:

$$P_{\mathrm{c}}(s)=P_{\mathrm{g}}-P_{\mathrm{l}}=\sigma\,\mathrm{Cos}\theta_{\mathrm{c}}\sqrt{\frac{\varepsilon}{K_{\mathrm{p}}}}F_{\mathrm{c}}(s). \tag{6}$$

In Eq. 6 $F_{\mathrm{c}}(\mathrm{s})$ is the Leverett function. For a hydrophilic porous medium: $\theta_{\mathrm{c}}<90°$. Addition of Eqs. 2 and 3 leads to:

$$\nabla\left(\boldsymbol{\upsilon}_{\mathbf{l}}+\boldsymbol{\upsilon}_{\mathbf{g}}\right)=\nabla\boldsymbol{\upsilon}=0. \tag{7}$$

By applying the gradient operator to both parts of the equality $P_{\mathrm{c}}(\mathrm{s})=P_{\mathrm{g}}-P_{\mathrm{l}}$, one obtains, after rearrangement:

$$\frac{1}{\lambda_{\mathrm{l}}+\lambda_{\mathrm{g}}}\frac{\mathrm{d}P_{\mathrm{c}}(s)}{\mathrm{d}s}\nabla s=\frac{\lambda_{\mathrm{l}}}{\lambda_{\mathrm{l}}+\lambda_{\mathrm{g}}}\boldsymbol{\upsilon}_l-\frac{\lambda_{\mathrm{g}}}{\lambda_{\mathrm{l}}+\lambda_{\mathrm{g}}}\boldsymbol{\upsilon}_g=\frac{\lambda_{\mathrm{l}}}{\lambda_{\mathrm{l}}+\lambda_{\mathrm{g}}}\boldsymbol{\upsilon}-\boldsymbol{\upsilon}_g. \tag{8}$$

By applying the gradient operator to both parts of equality (8) and using the equation of the conservation of the total phase-velocity $\boldsymbol{\upsilon}$ (7), one obtains:

$$-\nabla\left(\frac{1}{\lambda_{\mathrm{l}}+\lambda_{\mathrm{g}}}\frac{\mathrm{d}P_{\mathrm{c}}(s)}{\mathrm{d}s}\nabla s\right)-\frac{\mathrm{d}}{\mathrm{d}s}\left(\frac{\lambda_{\mathrm{l}}}{\lambda_{\mathrm{l}}+\lambda_{\mathrm{g}}}\right)\boldsymbol{\upsilon}\nabla s=0. \tag{9}$$

As a result, the system of equations describing the transport of liquid and gas phases across the current collectors (considered as a homogeneous and hydrophilic porous medium) is:

$$\begin{cases}-\nabla\left(\frac{1}{\lambda_{\mathrm{l}}+\lambda_{\mathrm{g}}}\frac{\mathrm{d}P_{\mathrm{c}}(s)}{\mathrm{d}s}\nabla s\right)-\frac{\mathrm{d}}{\mathrm{d}s}\left(\frac{\lambda_{\mathrm{l}}}{\lambda_{\mathrm{l}}+\lambda_{\mathrm{g}}}\right)\boldsymbol{\upsilon}\nabla s=0\\ \nabla\boldsymbol{\upsilon}=0\\ \boldsymbol{\upsilon}_{\mathrm{g}}=\frac{\lambda_{\mathrm{l}}}{\lambda_{\mathrm{l}}+\lambda_{\mathrm{g}}}\boldsymbol{\upsilon}-\frac{1}{\lambda_{\mathrm{l}}+\lambda_{\mathrm{g}}}\frac{\mathrm{d}P_{\mathrm{c}}(s)}{\mathrm{d}s}\nabla s\end{cases}. \tag{10}$$

The first term of Eq. 10 has the form of a diffusion equation: $\nabla[D_s(s)\nabla s]-\boldsymbol{\upsilon}_s\nabla s=0$. Here $D_s(s)=-\frac{1}{\lambda_{\mathrm{l}}+\lambda_{\mathrm{g}}}\frac{\mathrm{d}P_{\mathrm{c}}(s)}{\mathrm{d}s}$ corresponds to a diffusion factor associated with the liquid phase. The term $\upsilon_s=\upsilon\frac{\mathrm{d}}{\mathrm{d}s}\left(\frac{\lambda_{\mathrm{l}}}{\lambda_{\mathrm{l}}+\lambda_{\mathrm{g}}}\right)$ corresponds to convective velocity. Equation 10 can be conveniently rewritten by using appropriate variables determining the total fluxes of gaseous and liquid phases. Let us note:

$$\begin{cases}N_{\mathrm{g}}=\boldsymbol{\upsilon}_{\mathrm{g}}C_{\mathrm{g}}\\ N=\frac{C_{\mathrm{g}}C_{\mathrm{l}}}{C_{\mathrm{g}}+C_{\mathrm{l}}}\boldsymbol{\upsilon}\end{cases}. \tag{11}$$

Then Eq. 10 can be rewritten as:

$$\begin{cases}-\nabla\left(\frac{1}{\lambda_{\mathrm{l}}+\lambda_{\mathrm{g}}}\frac{\mathrm{d}P_{\mathrm{c}}(s)}{\mathrm{d}s}\nabla s\right)-\frac{C_{\mathrm{g}}+C_{\mathrm{l}}}{C_{\mathrm{g}}C_{\mathrm{l}}}\frac{\mathrm{d}}{\mathrm{d}s}\left(\frac{\lambda_{\mathrm{l}}}{\lambda_{\mathrm{l}}+\lambda_{\mathrm{g}}}\right)N\nabla s=0\\ \nabla N=0\\ N_g=\frac{C_{\mathrm{g}}+C_{\mathrm{l}}}{C_{\mathrm{l}}}\frac{\lambda_{\mathrm{l}}}{\lambda_{\mathrm{l}}+\lambda_{\mathrm{g}}}N-\frac{C_{\mathrm{g}}}{\lambda_{\mathrm{l}}+\lambda_{\mathrm{g}}}\frac{\mathrm{d}P_{\mathrm{c}}(s)}{\mathrm{d}s}\nabla s\end{cases} \tag{12}$$

2.4 Boundary conditions

Boundary conditions associated with Eq. 12 are:

(1) at the interface between current collector and flow channel, the saturation (the ratio between the volume of liquid to volume of pores) value is used;
(2) at the interface between current collector and the catalytic layer, the boundary condition for the flow of gas and liquid phase are given in the following form:

$$\begin{cases} N_{ga} = \frac{i-i_p}{4F}\frac{1}{1-\tau} \\ N_{la} = -\frac{i}{2F}\left(1+2n_p\right) - \frac{i-i_p}{4F}\frac{\tau}{1-\tau} \quad \tau = \frac{P_s}{P} \\ N_{gc} = \frac{i-i_p}{2F}\frac{1}{1-\tau} \quad N_l = N + \left(N - N_g\right)\frac{C_l}{C_g} \\ N_{lc} = \frac{i}{F}n_p + \frac{i-i_p}{2F}\frac{\tau}{1-\tau}. \end{cases} \tag{13}$$

Boundary conditions (13) take into account the presence of a parasitic current density i_p which does not lead to the formation of oxygen and hydrogen, and assume that hydrogen and oxygen gases formed during electrolysis are saturated with water vapor. When setting the boundary condition between porous current collector and flow channels, it is assumed that the capillary pressure in the porous medium of the current collector is equal to the pressure in the gas bubble. The method used to calculate the critical dimension of the gas bubble and the saturation value at the interface between current collector and flow channel is described in the next section as well as hydrogen and oxygen crossover phenomena, due to the permeability of the SPE.

2.4.1 *Description and analysis of gases crossover phenomena*

Hydrogen crosspermeation phenomena across the SPE come from the fact that its solubility in the solid polymer electrolyte is not zero. Therefore, molecular hydrogen diffuses from the cathodic compartment of the electrolytic cell through the membrane up to the anodic catalytic layer where it is either reoxidized into protons according to:

$$H_2 \rightarrow H^+ + H^+ + 2e^- \tag{14}$$

or released with oxygen after transport through the porous anode. Since the potential of the anode during water electrolysis is high (between +1.5 and +2.0 V/NHE), a value such that reaction (14) is fast, and the model assumes that all diffusion hydrogen are recombinated into protons. However, in a practice, sometimes is experimentally observed that some amount of hydrogen molecules being able to leak out of the SPE through the porous anode to contaminate the oxygen production. The proportion of hydrogen molecules reaching the anode which are oxidized back into proton depends on operating parameters such as potential, temperature and current density [18], but also very markedly on the micro-structure of the catalyst-SPE interface (other possibility of hydrogen appearance in oxygen is corrosion phenomena have never been clearly put into evidence). For example, when catalyst particles are located inside the polymer matrix, several microns below the membrane surface (this is obtained when the electrode is plated onto the SPE using an impregnation-reduction method such as the one described in [4]), the roughness factor of the electrode is large and the proportion of hydrogen molecules released in oxygen is significantly low. On the contrary, when electrodes having low roughness factors are used, the proportion is larger. Whatever this proportion, both phenomena are detrimental to the efficiency of the process: H_2 found on the anodic side in the gas phase can react with O_2, leading to water and heat, and protons formed at the anode according to (14) migrate back to the cathode and as a result, this leads to the onset of a parasitic current of protons. This current which does not lead to the formation of hydrogen produce an increase in the potential of electrolytic cell due to the additional ohmic losses in the membrane. Therefore, the electricity used to split water molecules which are then re-obtained is dissipated as heat in the PEM cell, leading to lower cell efficiencies.

Oxygen diffuses through the membrane, from the anode to the cathode, in a similar way. In the cathodic catalytic layer the following electrochemical reaction takes place:

$$4H^+ + 4e^- + O_2 \rightarrow 2H_2O \tag{15}$$

During water electrolysis, the potential of the cathode is such that reaction (15) is potentially fast although lower than reaction (14). Again, the micro-structure of the catalyst-SPE interface is responsible for the amount of oxygen which is reduced back into water. As a result, a proportion of the protons drift does not lead to the formation of hydrogen, but is used for the reduction of diffusing oxygen. This process produce an increase of the potential of the electrolytic cell due to the additional ohmic losses in the membrane and to an increase of the cathodic overvoltage due to the formation of 4 additional protons, which subsequently do not form hydrogen. In the following, it will be considered that all cross-permeating molecules reaching the opposite electrode are re-oxidized (H_2) or reduced (O_2). This is a simplifying assumption because our purpose was not to model contamination levels but to evaluate current inefficiencies associated with the parasitic formation of water from H_2 and O_2 obtained by electrolysis.

Cross-permeation of hydrogen and oxygen through the membrane takes place according to two different processes: (i) diffusion; (ii) convective transfer of dissolved hydrogen and oxygen in water molecules involved in the

electrical osmosis drag. In the case of hydrogen transport, the convection flow of water through the membrane is opposite to the hydrogen diffusion flow. The total hydrogen flow through the membrane Q_{HM} does not depend on coordinates, and as a result it can be expressed as follows:

$$\begin{cases} Q_{HM} = -D_{HM}\frac{dC_H}{dy} + \upsilon_c \Gamma_H C_H = \text{const} & 0 < y < h_m \\ y = 0 \quad C_H = C_g & y = h_m \quad C_H = 0. \end{cases} \tag{16}$$

In Eq. 16 υ_c (the convective velocity of water through the membrane caused by electroosmosis), can be expressed as follows:

$$\upsilon_c = -\frac{i_\Sigma n_p}{FC_l}. \tag{17}$$

Equation 16 contains two unknown values (hydrogen concentration C_H and total hydrogen fluxes through the membrane Q_{HM}). Also, Eq. 16 is a first order equation, although it has two boundary conditions. Thus, the problem has a unique solution, which can be expressed as:

$$\begin{cases} C_H = C_g \dfrac{\exp\left[\frac{i_\Sigma n_p \Gamma_H}{FC_l D_{HM}}(h_m - y)\right] - 1}{\exp\left[\frac{i_\Sigma n_p \Gamma_H}{FC_l D_{HM}} h_m\right] - 1} \\ Q_{HM} = C_g \dfrac{i_\Sigma n_p \Gamma_H}{FC_l} \dfrac{1}{\exp\left[\frac{i_\Sigma n_p \Gamma_H}{FC_l D_{HM}} h_m\right] - 1}. \end{cases} \tag{18}$$

The value of the parasitic current density due to the hydrogen crossover i_{pH} is given by:

$$i_{pH} = 2FQ_{HM} = 2n_p \frac{C_g \Gamma_H}{C_l} \frac{i_\Sigma}{\exp\left[\frac{i_\Sigma n_p \Gamma_H}{FC_l D_{HM}} h_m\right] - 1}. \tag{19}$$

The convective flow of water across the membrane down to the cathode also promotes the diffusion of oxygen from the anode to the cathode. The total oxygen flux across the membrane can be calculated as discussed above for hydrogen. The only difference comes from the relative direction of the convective velocity υ_c which is now opposite. The solution for the transport of oxygen Q_{OM}, similar to Eq. 16 for hydrogen, is:

$$\begin{cases} C_O = C_g \dfrac{1 - \exp\left[-\frac{i_\Sigma n_p \Gamma_O}{FC_l D_{OM}}(h_m - y)\right]}{1 - \exp\left[-\frac{i_\Sigma n_p \Gamma_O}{FC_l D_{OM}} h_m\right]} \\ Q_{OM} = C_g \frac{i_\Sigma n_p \Gamma_O}{FC_l} \dfrac{1}{1 - \exp\left[-\frac{i_\Sigma n_p \Gamma_O}{FC_l D_{OM}} h_m\right]} \end{cases} \tag{20}$$

According to reaction (15), four electrons are required to obtain the recombination of one molecule of oxygen. Therefore, the value of the parasitic current density due to the oxygen crossover i_{pO} is given by:

$$i_{pO} = 4FQ_{OM} = 4n_p \frac{C_g \Gamma_O}{C_l} \frac{i_\Sigma}{1 - \exp\left[-\frac{i_\Sigma n_p \Gamma_O}{FC_l D_{OM}} h_m\right]}. \tag{21}$$

Thus, the resulting current density i_Σ is the sum of 3 different contributions:

$$i_\Sigma = i_0 + i_{pO} + i_{pH}, \tag{22}$$

where i_0 denotes the useful current density associated with water electrolysis. Membrane permeability to hydrogen and oxygen is such that the value of the current efficiency η_i is less than unity. Expressions of current density i_Σ and current density i_0 (corresponding to the rate of hydrogen and oxygen generation) are related through the following relationship:

$$1 - \eta_i = \frac{i_\Sigma - i_0}{i_\Sigma} = n_p \frac{C_g}{C_l} \left(4\Gamma_O \frac{1}{1 - \exp\left[-\frac{i_\Sigma n_p \Gamma_O}{FC_l D_{OM}} h_m\right]} + 2\Gamma_H \frac{1}{\exp\left[\frac{i_\Sigma n_p \Gamma_H}{FC_l D_{HM}} h_m\right] - 1} \right). \tag{23}$$

At small current densities, i_Σ from Eq. 23 takes the form:

$$1 - \eta_i = \frac{i_\Sigma - i_0}{i_\Sigma} = \frac{FC_g}{i_\Sigma h_m}(4D_{OM} + 2D_{HM}). \tag{24}$$

It follows from Eq. 24 that, at low current densities, even when there is not net production of hydrogen and oxygen, a parasitic current can exist (due to the presence of hydrogen in the cathodic channels and of oxygen in the anodic channels). Therefore, the current is equal to zero. At high current densities, Eq. 23 takes the form:

$$\frac{i_\Sigma - i_0}{i_\Sigma} = 4n_p \frac{C_g \Gamma_O}{C_l} \tag{25}$$

It follows from Eq. 25 that the value of current is constant at high operating current densities.

2.4.2 *Dimensions of gas bubbles at the current collector–flow channel interface*

The release of gas bubbles at the current collector–flow channel interface results from the combined action of several factors, the main of which being the resisting force to water flow. At high pressures, other factors can be neglected. To calculate the resisting forces, it is necessary to take into account the heterogeneous distribution of water velocity $\upsilon(y)$ at the surface of current collectors. The classical analytic expression obtained for laminar flows can be used for that purpose:

$$\upsilon(y) = 6\,\upsilon_0 \frac{y\,(h_{fc} - y)}{h_{fc}^2} \approx 6\frac{\upsilon_0}{h_{fc}} y, \tag{26}$$

where y ($0 \le y \le h_{fc}$) is the transverse coordinate along the flow channel. In Eq. 26 the approximation comes from the assumption that the radius of a gas bubble R_{bc} is small compared with the size of channel h_{fc}. In this case, it is assumed that the drag force is equivalent to a force at a certain constant average velocity U_{av}. U_{av} is the normalized integral of the velocity with the weight, equal to the transverse size of the gas bubble, at a distance y away from the surface of the current collector:

$$U_{av} = \frac{\int_0^{2R_{bc}} \sqrt{2yR_{bc} - y^2}\upsilon(y)\mathrm{d}y}{\int_0^{2R_{bc}} \sqrt{2yR_{bc} - y^2}\mathrm{d}y} = \frac{3}{2}\frac{\upsilon_0 R_{bc}}{h_{fc}}. \quad (27)$$

The radius of a gas bubble R_{bc} released at the surface of the current collector is determined by equating the expression of the drag force with the expression of the force of the surface tension F_σ:

$$F_\sigma = 2\pi\sigma \sin\theta R_p. \quad (28)$$

The force of surface tension is directed antiparallel to the vector associated with the sum of all forces which are acting to release gas bubbles. The contact angle θ_c is determined from the condition of wettability of the surface. The drag force F_U is determined by specific resistance, expressed through the Reynolds number and factor of resistivity ζ_U:

$$F_U = \frac{12\pi}{\mathrm{Re}}\varsigma_U \rho_l U_{av}^2 R_{bc}^2. \quad (29)$$

By equating Eqs. 29 and 28, one obtain:

$$R_{bc} = \sqrt{\frac{h_{fc}\sigma R_p \sin\theta_c}{18\mu_l \upsilon_0}}. \quad (30)$$

The pressure due to the surface tension P_{st} in a bubble having the critical dimension is given by:

$$P_{st} = \frac{2\sigma}{R_{bc}} = \sqrt{\frac{72\mu_l \upsilon_0 \sigma}{h_{fc} R_p \sin\theta_c}}. \quad (31)$$

The capillary pressure P_c in the porous current collector, which is assumed to be a hydrophilic medium, is determined from the Leverett function:

$$P_c = \sigma \cos\theta_c \sqrt{\frac{\varepsilon}{K_p}} F_c(1 - s_{fc}) \approx 1.472(1 - s_{fc})\,\sigma \cos\theta_c \sqrt{\frac{\varepsilon}{K_p}}. \quad (32)$$

In Eq. 32, only the linear part of the usual Leverett formula is considered. This is because it is assumed that the value of saturation is close to unity. By equating Eqs. 31 and 32 for the pressures, one obtain (for the anodic and cathodic channels):

$$1 - s_{fc} = 11.972 \sqrt{\frac{K_p \mu_l \upsilon_0}{\varepsilon h_{fc} R_p \sigma \sin\theta \cos^2\theta_c}}. \quad (33)$$

The physical meaning of Eq. 33 is that the saturation value inside the porous current collectors is mostly determined by the velocity of the water flow inside the flow channel. If the flow of water is larger than what is strictly needed for electrolysis (for example for cooling the electrolysis stack during operation), then the optimum value of the velocity of water flow should not be set any empirical value but more precisely determined by calculating accurately the amount of heat produced inside the electrolyser (which in turn is a function of operating current density and cell efficiency). When these two criteria are used for determining the water flow, undesirable saturation effects inside current collectors are limited and higher efficiencies can be obtained.

2.4.3 *Calculation of gas content inside current collectors near the current collector–catalytic layer interfaces*

It is now necessary to express the gas concentration at the interfaces between current collectors and catalytic layers. The mass-transfer equation of two-phase mixtures (12) can be solved and expressed as quadratures in the case of the one-dimension approximation. It can be assumed that the void fraction of the gas phase in the porous current collector is negligible at large operating pressures because the volume of the gas phase significantly decreases with pressure. Therefore, the resistance induced by the gas phase to the motion of the liquid phase can be neglected. Also, as discussed above, only the linear part of the Leverett function is used in the calculation. Using all these simplifying assumptions, motion equations can be written as:

$$\frac{\mathrm{d}P_c}{\mathrm{d}y} = \sigma \cos\Theta_c \sqrt{\frac{\varepsilon}{K_p}} \frac{\mathrm{d}F_c(s)}{\mathrm{d}s}\frac{\mathrm{d}s}{\mathrm{d}y} \approx -1.417\,\sigma \cos\Theta_c \sqrt{\frac{\varepsilon}{K_p}}\frac{\mathrm{d}s}{\mathrm{d}y} = -K_p^{-1}\frac{\mu_g N_g}{C_g(1-s)^3}, \quad (34)$$

where y is the transverse coordinate along the current collector ($0 < y < h$); N_g is the oxygen flow $\left(N_g = \frac{i}{4F}\right)$ or hydrogen flow $\left(N_g = \frac{i}{2F}\right)$.

To obtain a solution, the first order Eq. 34 requires one boundary condition. This condition is obtained at the interface between the catalytic layer and the flow channel:

$$y = 0 \quad s = s_{fc} \quad (35)$$

Equation 34 is then solved as a quadrature. Its solution in the case of the hydrogen transport through the cathodic current collector takes the following form:

$$1 - s_{cl} = \left[(1 - s_{fc})^4 + \frac{1.411\, h\, \mu_H\, i}{F\, C_g \sigma\, \cos\theta_c \sqrt{\varepsilon K_p}} \right]^{1/4}. \quad (36)$$

In a similar way, oxygen transport through the anodic current collector takes the following form:

$$1 - s_{cl} = \left[(1 - s_{fc})^4 + \frac{0.706\, h\, \mu_o\, i}{F\, C_g \sigma\, \cos\theta_c \sqrt{\varepsilon K_p}} \right]^{1/4}. \quad (37)$$

2.4.4 Heat production during water electrolysis

Heat production in the PEM cells (W_{MEA} per one cell in J) is determined by considering three main operating parameters: (i) the thermoneutral voltage E_{tn}, (ii) the operating voltage U_{cell} and (iii) the current density i_Σ in the electrolysis cell. The expression of W_{MEA} is given by:

$$W_{MEA} = i_\Sigma S_{MEA}(U_{cell} - E_{tn}), \quad (38)$$

where S_{MEA} is active area of electrolysis cell.

The mass flow of cooling water Q_{cl} circulating inside the flow channels is usually chosen to insure a uniform temperature inside the electrolysis cells. The uniformity of temperature can be checked by measuring the difference of temperature (ΔT) between inlet and output channels of the PEM cells or electrolysis stack. Because of the thermal conductivity of the different components of a PEM cell (SPE, catalysts, current collectors, bipolar plates), heat is released symmetrically by the cooling water circulating in the anodic and cathodic channels. Q_{cl} can be determined from the following simple expression:

$$Q_{cl} = \frac{W_{MEA}}{2C_{pw}\Delta T} = \frac{i_\Sigma S_{MEA}(U_{cell} - E_{tn})}{2C_{pw}\Delta T}. \quad (39)$$

From Eq. 39, it is then possible to calculate the value of the average water velocity v_0 in the flow channels:

$$v_0 = \frac{Q_{cl}}{h_{fc} D_{MEA} \rho_l} = \frac{i_\Sigma S_{MEA}(U_{cell} - E_{tn})}{2C_{pw}\Delta T h_{fc} D_{MEA} \rho_l}, \quad (40)$$

where ρ_l is the density of liquid water. The accurate calculation of the heat produced in the PEM cells or electrolysis stacks requires the determination of the current–voltage characteristic of the electrolysis cell. At any given current density, the cell voltage is the sum of different terms: (i) the reversible equilibrium potential of water decomposition, (ii) ohmic losses in the membrane (U_{rm}), in the current collectors, in the catalytic layers and in the structural elements of MEA (U_k) and (iii) the overvoltages associated with the activation of anodic and cathodic electrochemical reaction η. Ohmic losses in the membrane are given by:

$$U_{rm} = \rho_m h_m i_\Sigma \quad (41)$$

Ohmic losses in catalytic layers expressed as voltage drop (U_{cl}) can be evaluated under the assumption that activation potential losses are approximately uniform over the layer thickness. Then, the average value of the proton current is equal to 50% of the total current i_Σ. Taking into account the porosity ε_{pcl} of the polymer phase inside the catalytic layers, it is possible to obtain an approximation of U_{cl}, using the classical Bruggermans correction:

$$U_{cl} = \frac{\rho_m h_{cl} i_\Sigma}{\varepsilon_{mcl}^{1.5}},$$

where h_{cl} is the thickness of the catalytic layer. Ohmic losses in the current collectors have been evaluated from experimental data: $U_k \approx 0.25\, U_{rm}$.

The expression of the anodic overvoltage has been obtained from experimental results. The following relationships has been used:

$$\eta_a = \frac{RT}{\alpha_a F} \ln\left(\frac{i_\Sigma}{i_{ex}}\right) \quad i_0^0 \approx 380\ \mathrm{A/m^2} \quad (42)$$

Finally, the general expression of the voltage–current relationship of the electrolysis cell based on Eqs. 41–42 is therefore:

$$U = E_p + 1.25\rho_m h_m i_\Sigma + \frac{RT}{\alpha_a F} \ln\left(\frac{i_\Sigma}{i_{ex}}\right) \quad (43)$$

3 Numerical results and discussion

Numerical values of main geometrical parameters used in the simulations are compiled in Table 1.

In Table 1, the contact angle of wetting θ is given for porous titanium. During electrolysis, there is a chemical and electrochemical oxidation of the titanium current collector and titanium oxides are formed at the surface. According to the literature (see, for example [19, 20]), and to our own results, the contact angle of wetting for such material is ca. 70°.

Table 1 Geometrical and operating parameters

Parameter	Value
Diameter of MEA active area	$D_{MEA} = 0.182$ m
Active surface area of MEA	$S_{MEA} = 0.026\ m^2$
Acceptable temperature difference in the PEM cell	$\Delta T = 3$ °C
Width of flow channel	$h_{fc} = 1.5$ mm
Width of current collector	$h = 1.0$ mm
Porosity of current collector	$\varepsilon = 0.4$
Permeability of current collector	$K_p = 1 \times 10^{-11}\ m^2$
Average dimension of current collector pores	$R_p = 1 \times 10^{-5}$ m
Wetting angle of current collector	$\theta = 70°$

3.1 Influence of hydrogen and oxygen crossover phenomena on the electrochemical performances of electrolysis cells

Relative current losses due to gas crossover phenomena as a function of temperature and current density, and as a function of pressure and current density, are plotted in Figs. 2 and 3 respectively. Calculations have been made for $h_m = 250$ μm. Continuous lines in the plots indicate constant temperature ($T = 100$ °C, Fig. 2) and constant pressure ($P = 13$ MPa, Fig. 3) values. From these calculations, it is possible to conclude that performing water electrolysis at low current density is not interesting because of resulting low current efficiencies. At 1 A cm^{-2}, the current efficiency (at $T = 100$ °C and $P = 13$ MPa) is still less than 90%. At 2 A cm^{-2}, the current efficiency increases up to 94%, an acceptable value from the viewpoint of power costs. An operating current density of 0.6 A cm^{-2} can be considered as a threshold value below which insufficient faradaic yields become unacceptable.

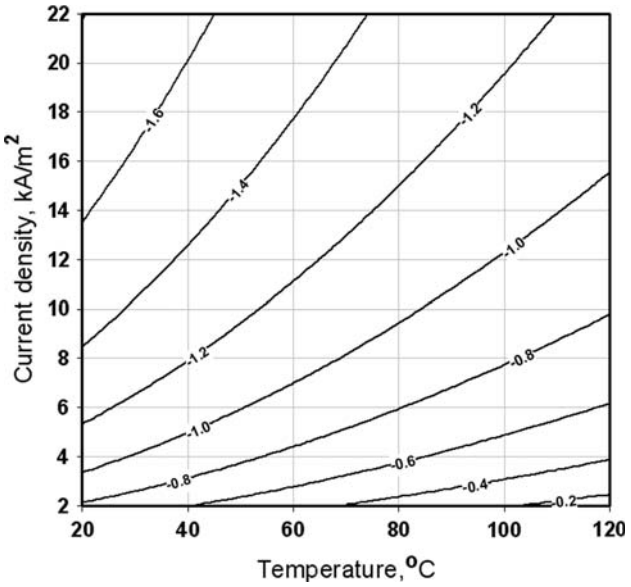

Fig. 2 Plots of the relative current losses (due to hydrogen and oxygen crossover) on a log scale as a function of operating temperature and current density ($P = 13$ MPa)

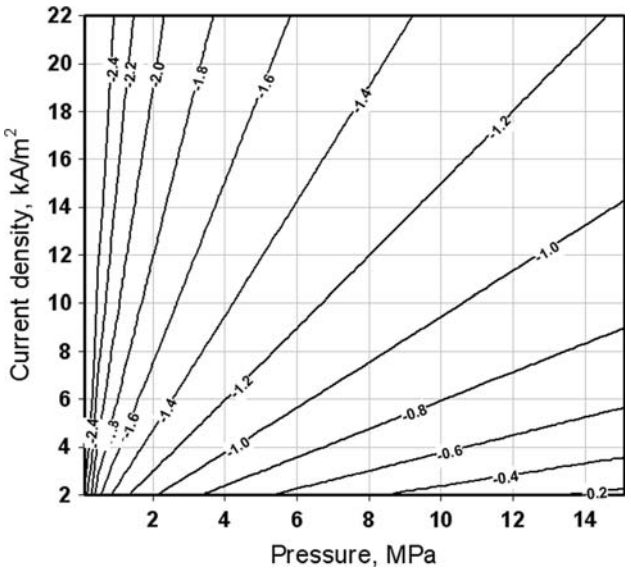

Fig. 3 Plots of the relative current losses (due to hydrogen and oxygen crossover) on a log scale as a function of operating pressure and current density ($T = 100$ °C)

3.2 Influence of membrane thickness on electrolysis cell performances

Dependences of the overall electrolysis cell efficiency on useful current density and membrane thickness are plotted in Fig. 4. The line of maximum efficiency is shown in bold. It is possible to conclude from the results of Fig. 4 that the optimum membrane thickness at a current density of 2 A cm^{-2} is 125μm, and 225 μm at a current density of 1 A cm^{-2}. The membrane thickness should be ca. 250–300 μm, a range for which the efficiency of the PEM cell slightly decreases when the membrane thickness increases.

3.3 Transport of two-phase mixtures across current collectors

The effect of operating temperature and current density on the relative volume of the gas phase in the porous current collector (i) near the flow channel and (ii) near the anodic

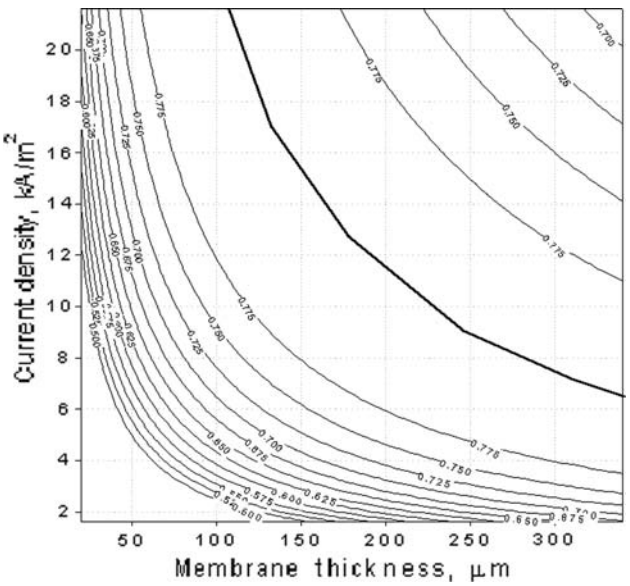

Fig. 4 Plots of overall electrolysis cell efficiency (rel.) as a function of useful current density and membrane thickness

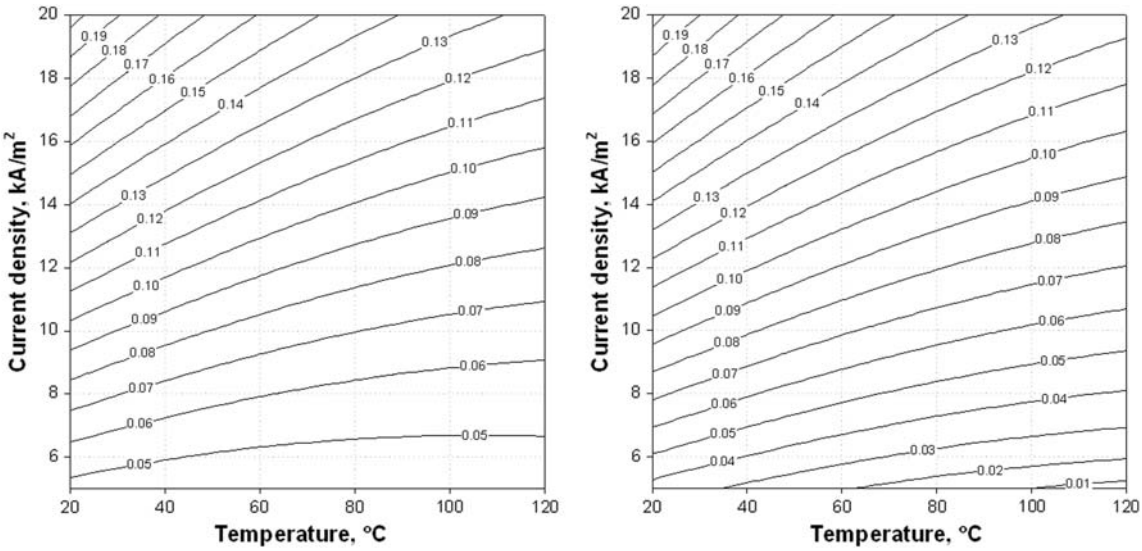

Fig. 5 Plots of the relative volume of the gas phase in the porous current collector near the anodic catalytic layer (*left*) and near the flow channel (*right*) as a function of operating temperature and current density ($P = 13$ MPa)

catalytic layer (at a constant pressure of 13 MPa) are shown in Fig. 5. Results were obtained from Eqs. 33 and 37. The temperature dependence of the saturation s is determined by the corresponding temperature dependence of fluid velocity υ_0. It can be seen that, at a current density of 1 A cm^{-2}, the volume of the gas phase inside the current collector, close to the interface between the current collector and the flow channel, is less than 10% of the volume of the liquid phase. Therefore, the current collector does not produce a significant resistance to the transport of the liquid–gas mixture, except in regions were the current density is less than 1 A cm^{-2}. As the current density decreases, the saturation increases and so does the resistance to the transport of the liquid phase.

The resistance to the transport of the biphasic mixture across the porous current collector decreases when the operating pressure increases. Therefore, it can be recommended to use current collectors with smaller porosity and smaller pores for operation at high pressure to reduce internal ohmic losses both in bulk regions and at the current collector–catalytic layer interfaces.

Using the above mentioned simplifying assumptions, the saturation of current collector near the flow channel is identical both on anodic and cathodic sides, and does not depend significantly upon operating pressure. Dependence on the specified factors takes place only in a saturation of a current collector far from the flow channel. When the water flow rate is reduced, the saturation of current collector increases. This is due to the fact that the size of gas bubbles coming off the current collectors is also increasing and that the pressure in such bubble decreases. As a result, the larger bubbles more effectively "pumps out" the gas from the current collector. With lower water flows, the effect proceeds as long as the separation of the bubble from the support is not determined by Archimedes forces.

3.4 Heat production

The calculated dependence of the thermal emission (W) of a circular PEM cell upon operating temperature and current density (at a constant pressure of 13 MPa) is plotted in Fig. 6. From these results, it can be concluded that heat produced during water electrolysis is inversely proportional to the operating temperature. This effect is due to the

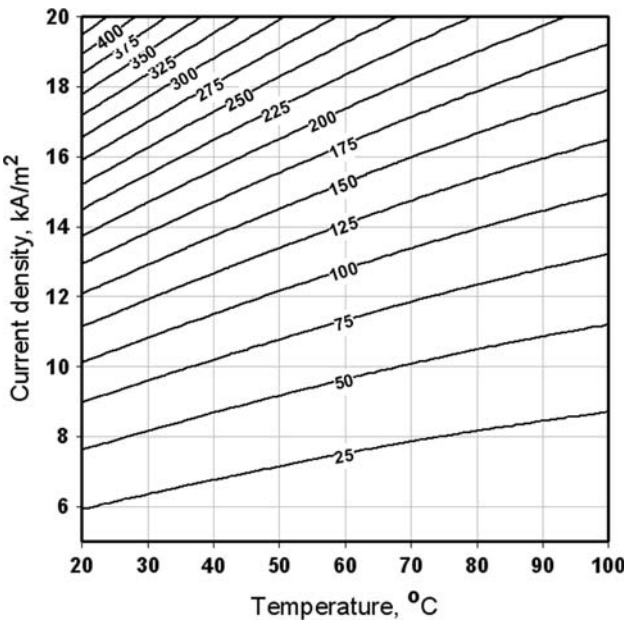

Fig. 6 Plots of heat (W) produced by a circular PEM cell as a function of operating temperature and current density ($P = 13$ MPa)

strong temperature dependence of the internal resistance of PEM cells.

Current density and activation losses at the anodes are not the only criteria to take into account to determine the value of the water flow across PEM cells. A second one, caused by the mass-transfer of two-phase (liquid–gas) mixtures across current collectors should also be considered. Usually, the value of the water mass flow is chosen to insure a uniform temperature at the surface of the MEAs. However, when the flow of water increases, the value of saturation in the porous current collectors decreases. This is due to the fact that the average size of gas bubbles leaving the current collectors also decreases, and pressure inside gas bubbles increases. As a result, the amount of water supplied to the anodic catalytic layers tends to inappropriately low, and voltage activation losses tend to increase. Therefore, from these results, it can be concluded that the criterion of temperature uniformity inside PEM cells should not be applied too strictly when calculating the optimum water flow. From the model, a value $\Delta T \approx 3$ °C is found sufficient to supply enough water to the catalytic layers and avoid efficiency losses due to saturation effects.

4 Conclusions

In this paper, a model is proposed to model a PEM water electrolyser and analyze its performances as a function of different geometrical and operating parameters. From the results of the simulations, it can be concluded that high-pressure water electrolysis at low current densities is not interesting because of the influence of hydrogen and oxygen crossover effects, leading to low current efficiencies. An operating current density of 0.6 A cm^{-2} has been determined as a threshold value (at 100 °C and a pressure of 13 MPa) below which the electrolyser should not be operated because of the significantly low faradaic efficiency. An operating current density in the 1–2 A cm^{-2} range is more acceptable from the viewpoint of power costs. By computing the relative volume of the gas phase in the current collectors as a function of different operating parameters, it is found that, when the rate of water in the flow channels is increased, the content of gases in the pores of current collectors and catalytic layers increases. This is an undesirable effect which potentially can lead to uneven distribution of current lines inside the PEM cells and to lower efficiencies. Therefore, a first criterion which should be used to determine the optimum rate of water flow inside the cells is to insure that enough water is supplied to the anodes. Taking into account as second criterion the amount of heat which is produced during electrolysis and which has to be removed from the cells, a temperature increase $\Delta T \approx 3$ °C has been identified has an optimum giving the most appropriate rate of water flow. Finally, it should be noted that the model presented in this paper for optimizing PEM water electrolysers can also be used to optimize the design of other electrochemical PEM systems such as PEM hydrogen compressors and PEM reversible cells.

Acknowledgments This work has been supported by the Federal Agency for Science and Innovations of the Russian Federation within the framework of the Federal Principal Scientific-Technical Programme "Researches and development on priority directions in development of scientific technological complex of Russia for 2007–2012" and by the Commission of the European Communities (6th Framework Programme, STREP project GenHyPEM no 019802). Financial support from the Global Energy International Prize Non-Profit Foundation (Grant no MG-2008/04/3) is also gratefully acknowledged.

References

1. Ren X, Gottesfeld S (2001) J Electrochem Soc 148(1):A87
2. Broka K, Ekdunge P (1997) J Appl Electrochem 27:117
3. Pasaogullari U, Wang CY (2004) J Electrochem Soc 151:A399
4. Millet P, Andolfatto F, Durand R (1996) Int J Hydrogen Energy 21:87
5. Grigoriev SA, Porembsky VI, Fateev VN (2006) Int J Hydrogen Energy 31:171
6. Ni M, Leung MKH, Leung DYC (2008) Energy Convers Manag 49:2748
7. Onda K, Murakami T, Hikosaka T, Kobayashi M, Notu R, Ito K (2002) J Electrochem Soc 149:A1069
8. Choi P, Bessarabov DG, Dattaa R (2004) Solid State Ion 175:535
9. Springer TE, Zawodzinski TA, Gottesfeld S (1991) J Electrochem Soc 138:2334
10. Springer TE, Wilson MS, Gottesfeld S (1993) J Electrochem Soc 140:3513
11. Nguyen T, White RE (1993) J Electrochem Soc 140:2178
12. He W, Yi JS, Nguyen TV (2000) AIChE J 46:2053
13. Wang ZH, Wang CY, Chen KS (2001) J Power Sources 94:40
14. You L, Liu H (2002) Int J Heat Mass Transfer 45:2277
15. Natarajan D, Nguyen TV (2001) J Electrochem Soc 148:A1324
16. Kaviany M (1999) Principles of heat transfer in porous media. Springer, New York
17. Wang CY, Cheng P (1997) Adv Heat Transfer 30:93
18. Grigoriev SA, Millet P, Korobtsev SV, Porembskiy VI, Pepic M, Etievant C, Puyenchet C, Fateev VN (2009) Int J Hydrogen Energy 34:5986
19. Tsyganov IA, Pozdnyakov AI, Richter E, Majtts MF (2007) Solid State Phys. Bull Nizhniy Novgorod Univ N.I. Lobachevsky 1:52 (in Russian)
20. Vasilev VV, Luchaninov AA, Strelnitsky VE, Tolstolutskaja GD, Kopanets IE, Sevidova EK, Kononenko VI (2005) Quest Nucl Sci Tech 3(86):167 (in Russian)